Accepted for publication in the *International Journal for Uncertainty Quantification* Jan. 2012

A HOLISTIC APPROACH TO UNCERTAINTY QUANTIFICATION WITH APPLICATION TO SUPERSONIC NOZZLE THRUST

Christopher J. Roy[*a] and Michael S. Balch[b]

[a] *Aerospace and Ocean Engineering Department*
Virginia Tech
215 Randolph Hall
Blacksburg, Virginia 24061 USA
cjroy@vt.edu

[b] *Applied Biomathematics*
100 North Country Road
Setauket, New York 11733 USA
michael@ramas.com

In modeling and simulation (M&S), we seek to predict the state of a system using a computer-based simulation of a differential equation-based model. In general, the inputs to the model may contain uncertainty due to inherent randomness (aleatory uncertainty), a lack of knowledge (epistemic uncertainty), or a combination of the two. In many practical cases, there is so little knowledge of a model input that it should be characterized as an interval, the weakest statement of knowledge. When some model inputs are probabilistic and others are intervals, segregated uncertainty propagation should be used. The resulting uncertainty structure on the M&S output can take the form of a cumulative distribution function with a finite width, i.e., a p-box. Implications of sampling over interval versus probabilistic uncertainties in the outer loop are discussed and examples are given showing the effects of the choice of uncertainty propagation and characterization methods. In addition to the uncertainties in model inputs, uncertainties also arise due to modeling deficiencies and numerically approximations. Modeling uncertainties can be reduced by performing additional experiments and numerical uncertainties can be reduced by using additional computational resources; thus both sources of uncertainty can be modeled as epistemic and can be characterized as intervals and included in the total predictive uncertainty by appropriately broadening the prediction p-box. A simple example is given for the M&S predictions of supersonic nozzle thrust which incorporates and quantifies all three sources of uncertainty.

1. INTRODUCTION

Modeling and simulation (M&S) play an important role in the analysis, design, and optimization of scientific and engineering systems. For the purposes of this article, we will restrict our discussion to models based on differential or integral equations and which require approximate numerical solutions (i.e., simulations). In the areas of science and engineering, we are increasingly moving towards risk-based or risk-informed decision making with a heavy reliance on M&S, where risk can be defined as the probability of occurrence times the resulting adverse consequence. In traditional M&S, a single deterministic simulation is performed and a factor of safety is added to the M&S output (i.e., the prediction). For example, if the maximum stress allowed on a structure is 250 MPa and a finite element analysis with a factor of safety of three predicts a maximum stress of 200 MPa, then the deterministic M&S predicts that the structure will not fail. However, such an approach cannot provide information about the probability of occurrence; either an event happens (probability of unity) or it does not (probability of zero). In order to be useful in the estimation of risk, M&S must be nondeterministic, where predictions in concert with their associated probability of occurrence are made. Quantification of the total uncertainty in a M&S prediction relies on three fundamental supporting activities: verification, validation, and uncertainty propagation. This article extends the framework proposed in [1, 2] by allowing advanced methods for propagating uncertainty beyond simple sampling techniques. It also demonstrates the dangers

of treating epistemic uncertainties as random variables and begins to address the difficult topic of dependencies between input uncertainties.

Since differential equation-based models rarely admit exact solutions for practical problems, approximate numerical solutions must be used. The characterization of the numerical approximation errors associated with a simulation is called verification [1,3,4,5]. It includes discretization error, iterative convergence error, and round-off error (i.e., solution verification) as well as errors due to algorithm inconsistencies and computer programming mistakes (i.e., code verification). Model form uncertainty is commonly estimated using model validation [1,4,5], which can be defined as the assessment of model accuracy by way of comparison of simulation results with experimental measurements. Model inputs include not only parameters used in the model of the system, but also data from the description of the surroundings (e.g., boundary conditions). In general the model inputs may have associated uncertainties, and these uncertainties must be propagated through the model in order to determine the resulting uncertainties in the system outputs we would like to predict. Additional details on verification and validation can be found in Refs. 1-5.

One of the main objectives of this paper is to broaden the traditional view of uncertainty quantification, which is often considered to be synonymous with uncertainty propagation, to include the additional sources of uncertainty that are quantified during verification and validation activities [1,2]. Another objective is to identify situations where uncertainties are more appropriately treated as intervals rather than as probabilistic values. When the uncertain model inputs include both probabilistic and interval representations, then it is important to propagate these uncertainties differently [6]. Two approaches to propagating combined probabilistic and interval uncertainty are discussed in detail.

2. TYPES OF UNCERTAINTY

This section discusses the different types of uncertainty classified according to their fundamental essence. In addition, some of the possible approaches for characterizing the different types of uncertainty are discussed.

2.1 Aleatory uncertainty

Aleatory uncertainty (also called irreducible uncertainty, stochastic uncertainty, or variability) is uncertainty due to inherent variation or randomness. Aleatory uncertainty is generally characterized probabilistically by either a probability density function (PDF) or a cumulative distribution function (CDF), the latter being simply the integral of the PDF from minus infinity up to the value of interest. An example of an aleatory uncertainty is a manufacturing process which produces parts that are nominally 0.5 meters long. Measurement of these parts will reveal that the actual length for any given part will be different than 0.5 meters. With a sufficiently large number of samples (i.e., information), both the form of the CDF and the parameters describing the distribution of the population can be determined. The aleatory uncertainty in the manufactured part can only be changed by modifying the manufacturing or quality control processes; however, for a given set of processes, the uncertainty due to manufacturing is considered irreducible.

2.2 Epistemic uncertainty

Epistemic uncertainty (also called reducible uncertainty or ignorance uncertainty) is uncertainty that arises due to a lack of knowledge on the part of the analyst conducting the M&S. If knowledge is added (through experiments, improved numerical approximations, expert opinion, higher fidelity physics modeling, etc.) then the uncertainty can be reduced. If sufficient knowledge (which costs time and resources) is added, then the epistemic uncertainty can, in principle, be eliminated. For example, a model input may be governed by a random process; however, if only one observation is available, then one has no information on the distribution, its parameters, or even whether or not the input is in fact random. By making additional observations, knowledge is added and the underlying random nature of the input can be

elucidated. With a sufficiently large number of samples, the epistemic uncertainty is eliminated and the model input can be treated as a purely aleatory uncertainty. Epistemic uncertainty often arises when one is forced to rely on expert opinion due to a dearth of data on a parameter. Approaches for maximizing the informational content derived from expert elicitation can be found in [7].

The manner in which a purely epistemic uncertainty is characterized should reflect the state of knowledge that one has about the parameter. When one has very little knowledge about the value of the parameter, then an interval representation (with no associated probability distribution) is the weakest statement that one can make about the value of a parameter. When some information is available, then a probability distribution representing the degree of belief of the analyst (as opposed to frequency of occurrence of an event in aleatory uncertainty) can be used [8]. Such belief functions are often one of the standard probability distributions (e.g., normal, log-normal, beta) or simpler ones (e.g., uniform, triangular). For cases where the parameter is known to be a random variable with a given distribution, but the parameters describing the distribution are not precisely known (e.g., due to insufficient data), then a mixed distribution may be appropriate (see below). In the case of conflicting information, other approaches are available such as fuzzy sets [9] or evidence theory [10].

2.3 Mixed uncertainty

In many cases, uncertain parameters will be a mixture of aleatory and epistemic uncertainties. One approach for characterizing mixed aleatory and epistemic uncertainty is a probability box (or p-box), which is similar to a CDF but with a finite width representing the epistemic uncertainty [11]. The two outer bounding CDFs reflect the aleatory uncertainty in the variable (see **FIG. 1**). The width of the p-box represents the range of parameter values that are possible for a given cumulative probability, whereas the height of the p-box represents the range of interval-valued cumulative probabilities associated with a given parameter value.

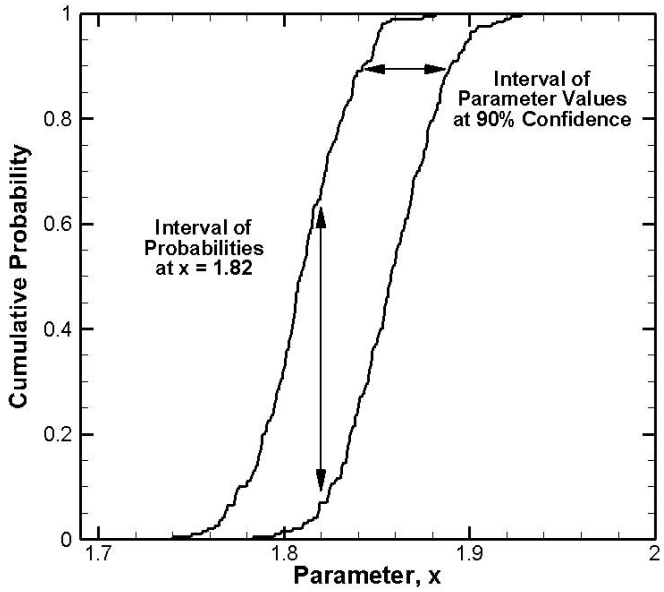

FIG. 1: Example probability box (p-box) for a parameter (x) that is a mixture of both aleatory (random) and epistemic (lack of knowledge) uncertainty.

Credal sets and Dempster-Shafer structures provide a more detailed way to represent mixed uncertainty. A credal set is a set of possible probability distributions [12]. It supports a belief function which, for a given set, returns the minimum level of probability accorded by the different probability

distributions in the credal-set. A Dempster-Shafer structure, on the other hand, is a collection of weighted sets, called focal elements, to which basic belief is assigned [10]. The belief for a set, *A*, is equal to the total combined weight of the focal elements contained in *A*. It is worthwhile to note that all Dempster-Shafer structures can be represented using credal sets, but there exist credal sets whose belief functions are not supported by any Dempster-Shafer structure [13]. Similarly, a p-box can be derived from a given credal set or a Dempster-Shafer structure. Given a credal set on a real-valued variable, a p-box is simply the minimum and maximum CDF values for the various probability distributions contained in the credal set. Given a Dempster-Shafer structure, the lower and upper bounds on the p-box are the cumulative belief and plausibility functions of said Dempster-Shafer structure [14].

3. SOURCES OF UNCERTAINTY

In M&S, we are interested in predicting the behavior of certain system outputs which we will refer to as system response quantities, or SRQs (sometimes referred to as quantities of interest). This section describes the three sources of uncertainty in M&S [1,2]: uncertainty in model inputs, uncertainty due to numerically solving (i.e., simulating) the model, and uncertainty due to imperfections in the model itself. Uncertainty propagation is used to determine the effects of model input uncertainties on the SRQs. Verification is the process used to quantify and reduce the uncertainty due to numerical approximations. Validation involves comparison of simulation outcomes to experimental data in order to estimate the model form uncertainty. An overview of the factors contributing to the total prediction uncertainty is shown graphically in **FIG. 2**. The M&S may have inputs that are deterministic, aleatory, epistemic, or a mixture of aleatory and epistemic, and the propagation of these uncertainties through the model (blue arrow) contributes to the total prediction uncertainty. The errors that occur when numerically approximating (i.e., simulating) the solution to the model also gives rise to additional uncertainties (red arrow). Finally, the model imperfections also contribute to the total prediction uncertainty (green arrow). The model form uncertainty is assessed through comparisons with experimental data and increases when it is extrapolated to conditions where no experimental data are available (i.e., the prediction conditions).

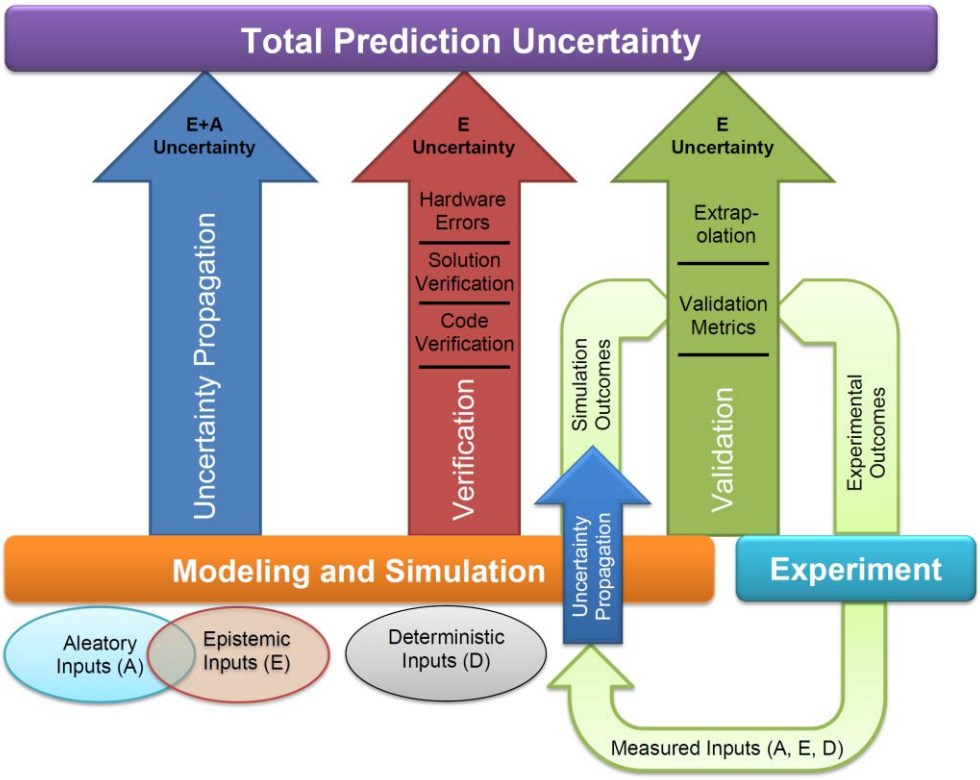

FIG. 2: Overview of the factors contributing to total prediction uncertainty.

3.1 Model input uncertainty

Model inputs include not only parameters used in the model of the system, but also data from the description of the surroundings (e.g., boundary conditions). Uncertainties in model inputs must be propagated through the model in order to determine their effects on the SRQs. The approach used for propagating uncertainty depends not only on the type of uncertainty, but also on the approach used for characterizing it. Here we discuss some possible approaches for propagating probabilistic, interval, and mixed probabilistic/interval uncertainty.

3.1.1 Probabilistic

Probabilistic representations for model inputs can arise from aleatory uncertainties or when belief functions are used to describe epistemic uncertainties. When there are only probabilistic model inputs, then there are a number of different approaches for propagating this uncertainty through the model. The simplest approach is Monte Carlo sampling, where inputs are sampled randomly from their probability distribution and then used to generate a sequence of SRQs. The problem with sampling is that it tends to converge slowly. For example, the mean value converges as $1/\sqrt{N}$ where N is the number of samples; low probability events and higher moments converge even slower [15]. Other approaches, such as Latin hypercube sampling, can show improved convergence properties in some cases. Perturbation methods can be used when 1) sensitivity derivatives of the SRQs with respect to the uncertain inputs are available and 2) the uncertainties in the inputs and the SRQs are small [16]. In polynomial chaos, the SRQ is expanded as a polynomial in terms of the uncertain model inputs. While initial polynomial chaos implementations were code intrusive [17], more recently non-intrusive forms of polynomial chaos have been developed (e.g., see [18]) based on spectral projection or point collocation. When only a few aleatory uncertain

variables are present (e.g., less than five or ten), then non-intrusive polynomial chaos has the potential to significantly reduce the number of samples required for statistical convergence of the CDF. For larger numbers of uncertain variables, more traditional sampling methods have proven to be more robust. When a response surface approximation of the SRQs as a function of the uncertain model inputs is available, then any of the sampling or non-intrusive methods discussed above can be computed efficiently.

3.1.2 Intervals

When all uncertain inputs are characterized by intervals, there are three main approaches for propagating the uncertainty to the SRQs. The simplest is sampling over the input intervals in order to estimate the interval bounds of the SRQs, and Latin hypercube sampling is recommended [19]. The propagation of interval uncertainty can also be formulated as a bound-constrained optimization problem: given the possible range of the interval uncertain inputs, determine the possible minimum and maximum values of the SRQs. Standard approaches for optimization such as local gradient-based searches and global search techniques can be used. Finally, interval arithmetic involves replacing floating point numbers in a simulation code with interval values and then redefining arithmetic operators and functions for intervals [9,20]. While naïve implementations can result in overly-conservative interval bounds on the SRQs, advanced techniques to provide tighter (and possibly rigorous) bounds on the interval output are an active area of research. An interval arithmetic toolbox also exists within the popular MATLAB© software [21].

3.1.3 Mixed probabilistic/intervals

When some model inputs are probabilistic and other are characterized with intervals, then additional approaches are needed for propagating the uncertainty through the model [6]. One method for propagating mixed interval and probabilistic uncertainty is segregated uncertainty propagation. This process can be described as consisting of an outer-loop and an inner-loop. On the outer-loop, samples from the interval-uncertain model inputs are drawn. For each of these sample-values, the probabilistically-uncertain model inputs are propagated along with the fixed sample-value of the interval-uncertain variable. This propagation of the probabilistic uncertainty is the inner-loop of segregated uncertainty propagation. The result of one of these steps is a possible probability distribution on the SRQ. The total result of the process will be a collection of possible probability distributions on the SRQ; that is, a credal set. Were the sampling to be exhaustive, this process would yield the correct solution for problems in which the interval-uncertain inputs had a stationary distribution and were independent of the probabilistic inputs [13]. An advantage of this segregated approach is that the inner aleatory propagation loop can be achieved using Monte-Carlo sampling or any of the advanced techniques described above for propagating probabilistic uncertainty (polynomial chaos, stochastic collocation, etc.).

An alternative method is to reverse the inner and outer loops. Under this approach, a random Monte-Carlo sample is drawn from the probabilistically represented model inputs. For each of the random outer-loop sample-values, the uncertainty on the interval-uncertain inputs is propagated. The result of one iteration of this inner loop is an interval on the output SRQ. The total result of the two-layer propagation process is a Dempster-Shafer structure [13]. For this case, the inner loop over the interval uncertainty can be achieved using sampling or one of the advanced techniques discussed above for propagating interval uncertainties (i.e., optimization or interval arithmetic).

Since p-boxes can be derived from credal sets and Dempster-Shafer structures, they provide common ground on which to represent mixed interval and probabilistic uncertainty. In this paper, the terms E-outer and A-outer p-box are used to differentiate results using the two segregated propagation methods described in the previous two paragraphs. The term E-outer p-box is used when a p-box was derived by propagating the interval uncertainty on the outer-loop because intervals represent epistemic uncertainty. The term A-outer p-box is used when a p-box was derived by propagating probabilistic uncertainty on the outer-loop because of the use of probability to represent aleatory uncertainty.

Despite the seeming similarity of the two segregated uncertainty propagation processes described above, the results they obtain can differ significantly. First of all, as already mentioned, the two processes result in different types of mathematical objects. The results obtained using either approach can be

expressed in the form of a p-box, but the A-outer and E-outer p-boxes for a given problem will not necessarily be the same. The reason is that the two approaches correspond to different states of knowledge about the dependence between the interval-uncertain inputs and the probabilistically uncertain inputs. If the interval-uncertain inputs are fixed unknown constants or stochastically independent of the aleatory-uncertain inputs, then E-outer propagation yields correct results [13]. For example, a fixed (unknown) bias uncertainty and a random uncertainty in an experimentally measured quantity are correctly combined using E-outer propagation. In contrast, if the dependence between the interval-uncertain and aleatory uncertain inputs is unknown, then A-outer propagation yields correct results [13]. For example, two parameters with unknown dependence had to be propagated in a recent study quantifying uncertainty in Mars atmosphere models [13]. Section 4 of this article explores A-outer and E-outer propagation in more detail and provides a concrete example of the dissimilar results that the two methods can yield.

3.2 Numerical uncertainty

The sources of numerical approximation error that can occur during the simulation of a model include discretization error, iterative error, round-off error, and errors due to coding mistakes [1]. Discretization error arises due to the fact that the spatial domain is decomposed into a finite number of nodes/elements and, for unsteady problems, time is advanced with a finite time step. Discretization error is difficult to estimate for practical problems and is often the largest of the numerical errors. Iterative convergence errors are present when the discretization of the model results in a simultaneous set of algebraic equations that are solved approximately or when relaxation techniques are used to obtain a steady-state solution. Round-off errors occur due to the fact that only a finite number of significant figures can be used to store floating point numbers in a digital computer. Finally, coding mistakes can occur when numerical algorithms are implemented into a software tool. Since coding mistakes are, by definition, unknown errors (they are generally eliminated when they are identified), their effects on the numerical solution are extremely difficult to estimate. For cases where numerical approximation errors can be estimated, their impact on the SRQs of interest can, in principle, be eliminated if sufficient computing resources are available. If this is not practical, they should generally be converted to epistemic uncertainties due to the uncertainties associated with the error estimation process itself. One of the simplest and most conservative methods for converting error estimates to uncertainties is to use the magnitude of the error estimate to apply uncertainty bands about the simulation prediction, possibly with an additional factor of safety included. For example, let f_h be the numerical solution, $\bar{\varepsilon}_h$ be the error estimate, and $\tilde{f}$ be the (unknown) true solution to the model. The estimated exact solution $\overline{f}$ is then given by $\overline{f} = f_h - \bar{\varepsilon}_h$ and the numerical uncertainty U due to the error estimation process can be approximated by

$$U = F_s \left| \bar{\varepsilon}_h \right| \tag{1}$$

where $F_s \geq 1$ is a factor of safety. The resulting interval for the solution, accounting for numerical uncertainties, can be given by

$$f_h \pm U = f_h \pm F_s \left| \bar{\varepsilon}_h \right| \tag{2}$$

These concepts are shown graphically in **FIG. 3** with a factor of safety of approximately $F_s = 1.5$. When the error estimate is poor (i.e., when the true model solution $\tilde{f}$ differs significantly from the estimated model solution $\overline{f}$), this approach is designed to still potentially provide conservative numerical uncertainty estimates, depending of course on the chosen factor of safety. It is recommended that this uncertainty be centered about the numerical solution f_h rather than the estimated model solution $\overline{f}$ since the latter can lead to erroneous (and possibly physically non-realizable) values. When multiple sources of

numerical error are present, then a conservative approach is to simply add the numerical uncertainties together [1,2], i.e.,

$$U_{\text{NUM}} = U_{\text{RoundOff}} + U_{\text{Iteration}} + U_{\text{Discretization}}. \tag{3}$$

While numerical approximation uncertainties are epistemic in nature, it is currently an open question as to whether these uncertainties should be characterized probabilistically or as intervals [22].

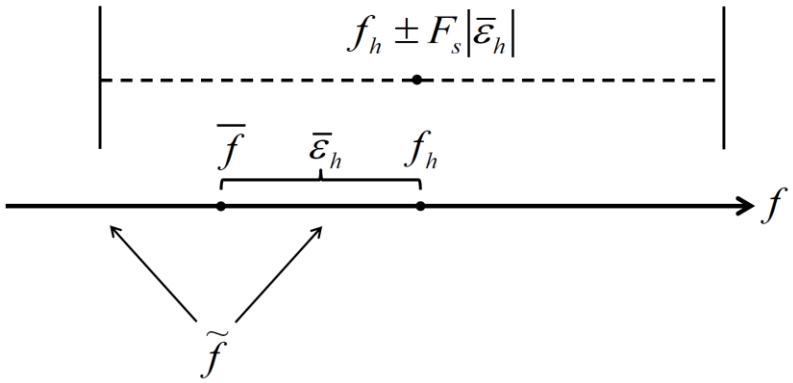

FIG. 3: Sketch showing the conversion of a numerical error estimate to an interval uncertainty.

3.3 Model form uncertainty

The estimation of model form uncertainty for an M&S prediction can be decomposed into two parts [1,23]. First, one statistically quantifies the disagreement between the simulation results and all of the conditions for which experimental measurements are available using a validation metric (i.e., a measure of the model form uncertainty). Second, this measured model form uncertainty is extrapolated to application conditions where the prediction is to be made (i.e., the conditions where no experimental data exist). These two aspects of model form uncertainty are described in detail below. It should be noted that this explicit treatment of model form uncertainty is an alternative to Bayesian model updating in which all available experimental data are used to update the model parameters and thus provide the best simulation prediction given the available information. See Refs. [1,2] for additional details.

A validation metric is a mathematical operator that requires two inputs: the experimental measurements of the SRQ of interest and the prediction of the SRQ at the conditions used in the experimental measurements. While there are many possible validation metrics, we will focus on one implementation called the area validation metric. When only aleatory uncertainties are present in the model inputs, then propagating these uncertainties through the model produces a CDF in the SRQ. Experimental measurements are then used to construct an empirical CDF of the SRQ. The area between these two CDFs is referred to as the area validation metric *d* (also called the Minkowski L_1 norm) and is given by

$$d(F, S_n) = \int_{-\infty}^{\infty} |F(x) - S_n(x)| dx \tag{4}$$

where *F(x)* is the CDF from the simulation, $S_n(x)$ the CDF from the experiment, and *x* is the SRQ. The area validation metric *d* has the same units as the SRQ and effectively provides a measure of the evidence for disagreement between the simulation and the experiment [23]. An example of this area validation metric for a case with only aleatory (i.e., probabilistic) uncertainty occurring in the model input

parameters is given in **FIG. 4**. In this figure, the aleatory uncertainties have been propagated through the model (e.g., with a large number of Monte Carlo samples), but only four experimental measurements are available. The stair-steps in the experimental measurements are the locations of each of the four experimental measurements. As a result, each measurement is assigned a probability of 0.25. The area validation metric is the area between the simulation CDF and the experimental CDF. While this validation metric does not distinguish between good agreement with limited data and poor agreement with rich data, it does have the desirable property that the validation metric will increase in both cases. This metric can also be computed for cases involving both aleatory and epistemic uncertainty in the model inputs (e.g., see Refs. 1 and 24).

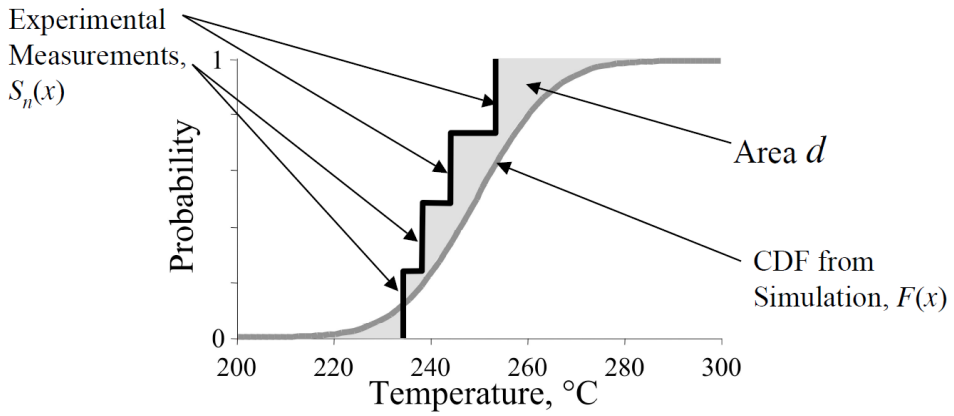

FIG. 4: Area validation metric example (reproduced from [23]).

The general process for determining the model form uncertainty at the conditions of interest (i.e., the prediction location) is as follows. First, a regression fit of the validation metric is performed in the space of the validation domain. Next, a statistical analysis is performed to compute the prediction interval at the conditions of interest. This prediction interval is similar to a confidence interval, but it will be larger because we are interested in a future random deviate predicted by the regression fit of the validation metric data, i.e., the uncertainty due to the regression fit and due to the variability of the validation metric evaluated at multiple conditions. The computation of the prediction interval requires a level of confidence to be specified (e.g., 95% confidence). The model form uncertainty at the prediction conditions is then found by taking the maximum of zero and the value found from the regression fit of the validation metric and adding in the upper value of the prediction interval. For example, if the value of the regression fit at the prediction condition is $\hat{d}$ and the 95% confidence interval is $\hat{d} \pm P$, then the model form uncertainty at that location is given by $\max(\hat{d},0) + P$. A detailed example showing the extrapolation of model form uncertainty will be given later in Section 5.3. This approach for extrapolating model form uncertainty does not account for the case where different physical phenomena occur at the prediction condition as compared to the validation conditions. In such cases, one may resort to expert elicitation [7] to estimate the increase or decrease in the uncertainty at the prediction location.

4. PROPAGATION OF MIXED UNCERTAINTY SOURCES

Since the segregated uncertainty propagation methods discussed in Section 3.1.3 are likely unfamiliar to most readers, it makes sense to preface Section 5 with some simple analytic examples of uncertainty propagation. Moreover, such examples can demonstrate the importance of propagating uncertainty correctly. Consider a problem in which variable X, which is uniform random from zero to one, must be propagated with variable Y, which is interval-uncertain on [0,1]. The functions $Z_1 = X+Y$ and $Z_2 = (X+Y-1)^2$ provide a test-bed for demonstrating the results of different joint representations of X and Y.

To find the lower and upper CDFs for Z_1 or Z_2, first map back to the set in (X,Y) space corresponding to the set $Z \leq z$. Such sets are marked in gray in **FIG. 5** for two example-values of z_1 and z_2. Since X is uniform random, lower and upper CDF values for the E-outer p-box are the minimum and maximum widths of the intersection between the gray sets and the line $Y=y$ taken over the set of possible y-values between zero and one. That is, the lower and upper CDF values using exhaustive E-outer sampling are the minimum and maximum possible probabilities for $Z \leq z$, given a fixed y-value. In calculating the A-outer p-box, the lower CDF bound is the width of the set of x-values for which the filament $(x,[0,1])$ is contained in the gray set. The upper CDF bound is the width of the set of x-values for which the filament (x,[0,1]) intersects the gray set. The bottom two panels of **FIG. 6** and **FIG. 7** illustrate the A-outer and E-outer p-boxes obtained for these two problems.

As mentioned in Section 3.1.3, the E-outer p-box corresponds to an assumption of independence between X and Y. (It is worthwhile to note that the assumption of independence is automatically satisfied if Y is assumed to have a fixed, though unknown, value.) The A-outer p-box corresponds to a complete lack of knowledge about the relationship between X and Y. Sometimes the A-outer and E-outer p-boxes will be equal or close to equal. This is the case for Z_1, as illustrated in **FIG. 6**. However, as illustrated in **FIG. 7**, that the A-outer and E-outer p-boxes do differ for Z_2, which was a fairly simple non-linear function of X and Y. This example demonstrates that A-outer and E-outer propagation, though consisting of similar components, are not interchangeable.

Another issue of importance in uncertainty propagation is the erroneous but prevalent practice of replacing interval uncertainties with supposedly equivalent probability distributions. In purely probabilistic approaches to uncertainty quantification, it has been traditional to replace an interval uncertainty with a uniform probability distribution on said interval. An alternative approach has been to replace interval uncertainty with a normal distribution with its 2.5^{th} and 97.5^{th} percentiles at the lower and upper bounds of the interval. (This approach has its roots in the mid-to-late twentieth century, during which random normally distributed errors were often represented with a simple central 95% confidence interval.) As shown in the top two panels of **FIG. 6** and **FIG. 7**, on the whole, these two probabilistic representations of Y attain similar representations of Z_1 and Z_2.

Even in the simple example problems presented here, the errors caused by replacing intervals with probability distributions are apparent. In the case of independence, the probabilistic representations of uncertainty on the output variables are much narrower than the E-outer p-box. In the case of unknown independence, a probabilist might attempt to bound the distribution on the output by computing results for both perfect and opposite dependence [25]; even then, the range of results are still far narrower than the A-outer p-box. In short, an interval has no traditional probabilistic equivalent.

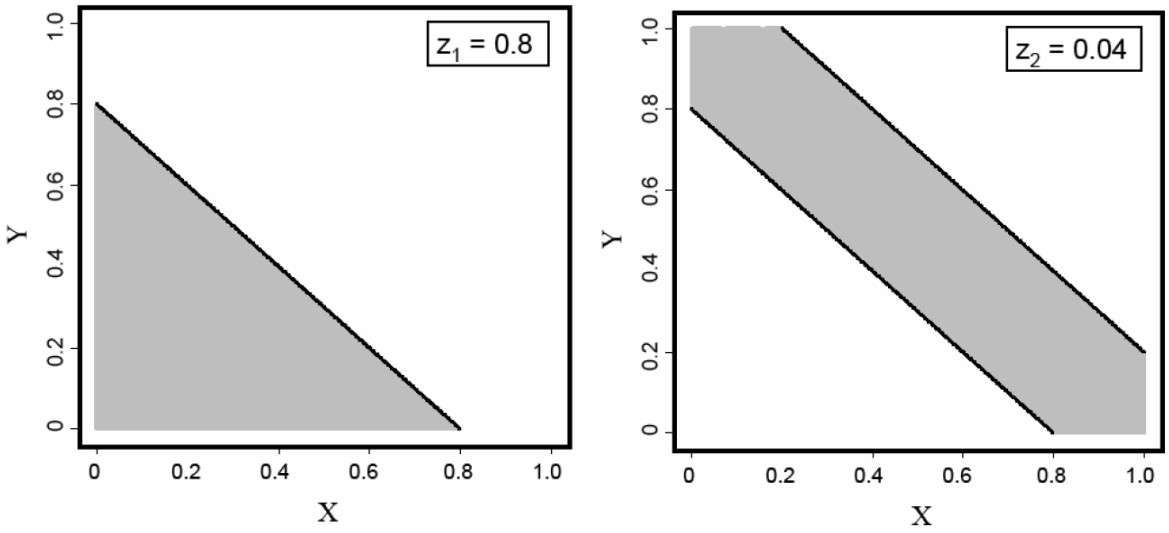

FIG. 5: Sets in the X-Y planes corresponding to sets $Z \leq z$.

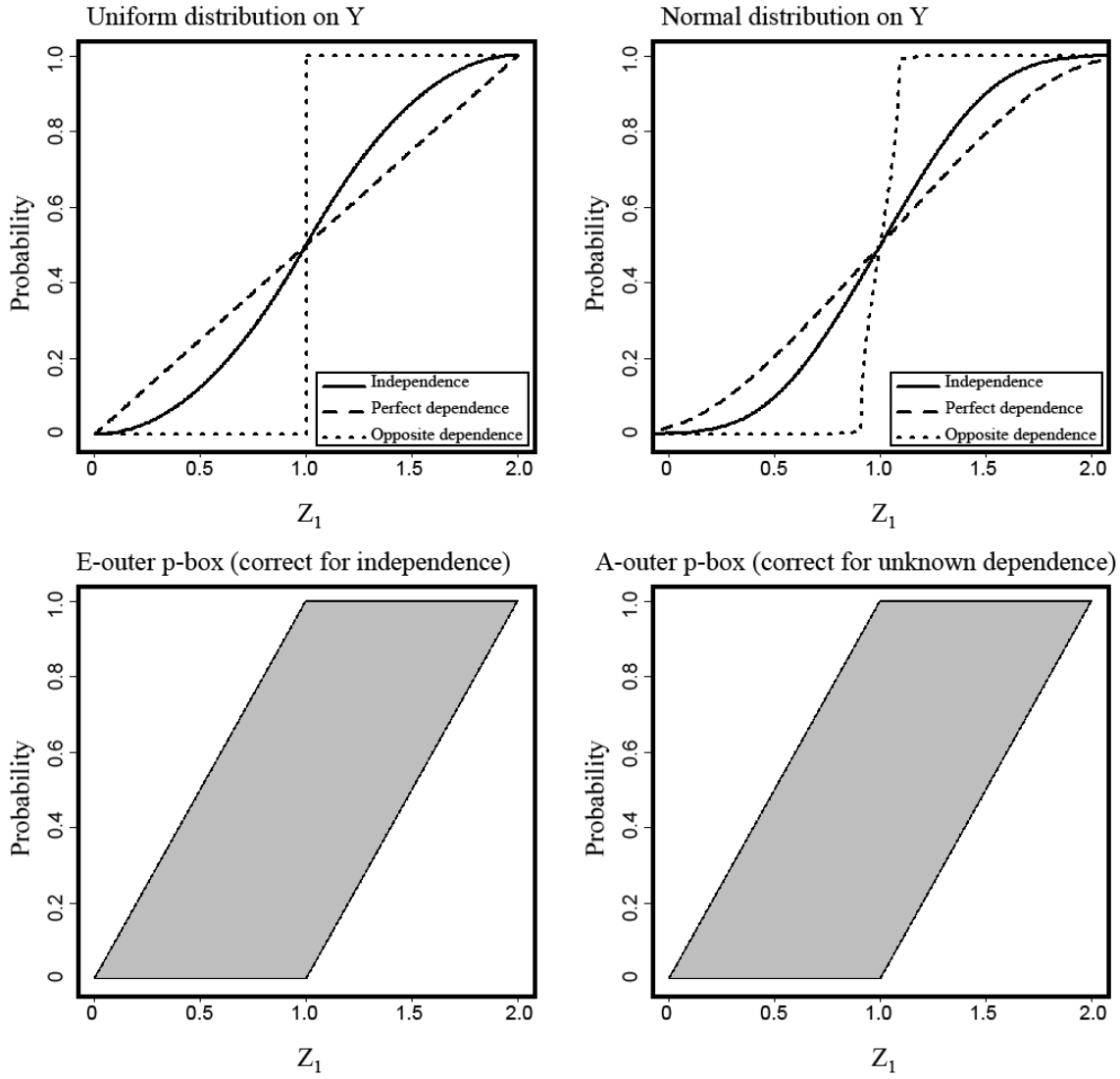

FIG. 6: Uncertainty in Z_1=X+Y given different treatments of Y.

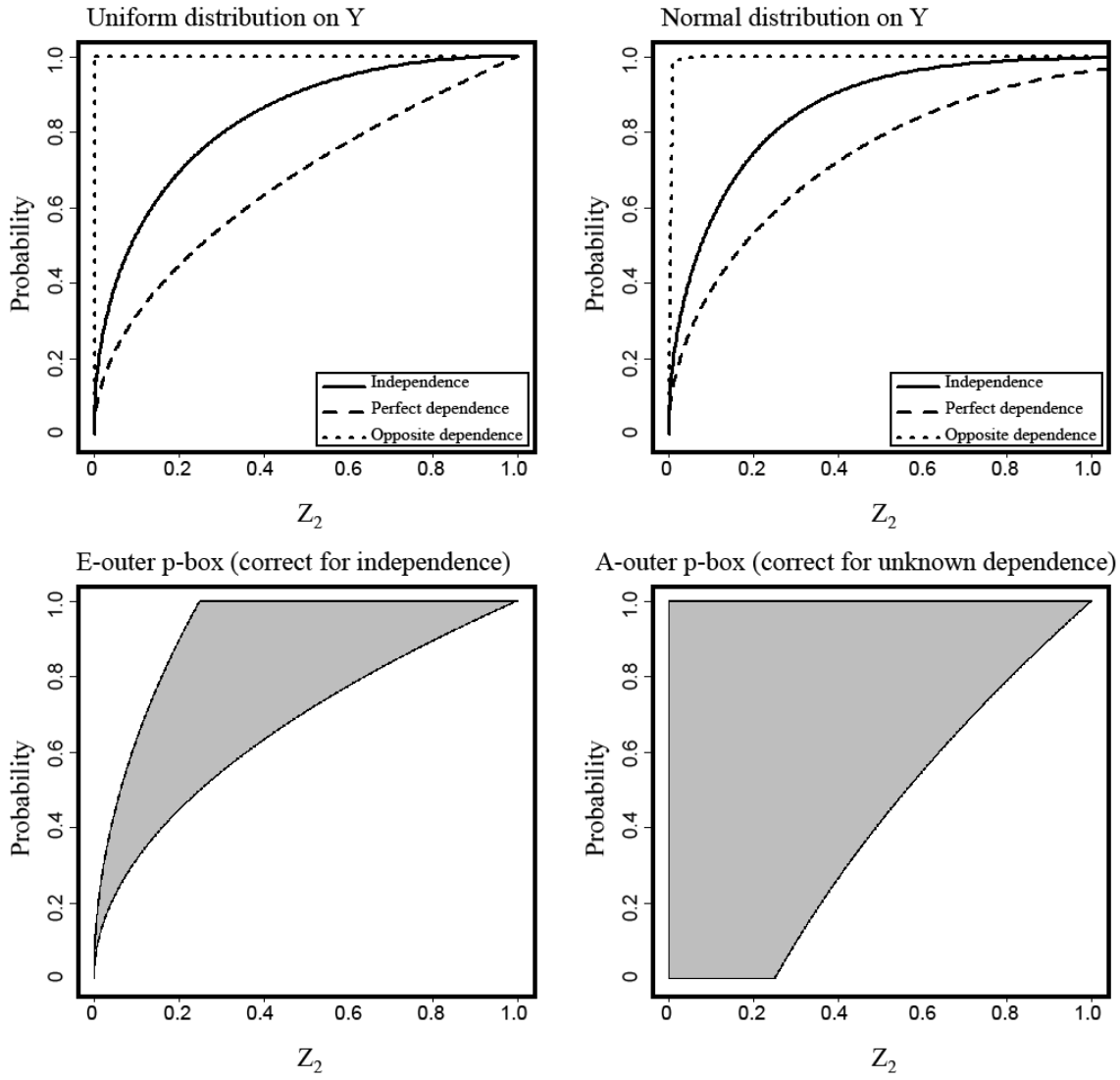

FIG. 7: Uncertainty in $Z_2=(X+Y-1)^2$ given different treatments of Y.

5. NOZZLE THRUST EXAMPLE

As a simple example of this holistic approach to uncertainty quantification, we consider the thrust produced by a supersonic nozzle. This nozzle is designed to achieve a nominal exit Mach number of approximately 2.5. The flow is modeled with the quasi-one-dimensional Euler equations which account for cross-sectional area variations in the nozzle. While the inviscid flow through a nozzle could be determined by simpler means (e.g., formulated as a set of boundary-value ordinary differential equations or even algebraic equations resulting from isentropic flow assumptions), we retain the more complex formulation in order to demonstrate all of the contributors to the total uncertainty in a M&S prediction. The weak (integral) form of the Euler equations is solved with a cell-centered finite volume formulation using a formally second-order accurate numerical scheme. Additional details of the problem setup can be found in [2]. All simulations are performed with 64 cells in the spatial direction unless otherwise noted.

The nozzle has a circular cross section with an effective radius (in meters) given by

$$r(x) = \begin{cases} 0.025 + 0.015\cos(\pi x / x_t) & x \le x_t \\ \dfrac{r_e + 0.01}{2} + \dfrac{0.01 - r_e}{2}\cos\left(\pi \dfrac{x - x_t}{2.5 - x_t}\right) & x > x_t \end{cases} \tag{5}$$

where $0 \le x \le 2.5$ m and the location of the nozzle throat is $x_t = 0.2$ m. The effective nozzle radius at the exit r_e depends on both the nozzle contour and the presence of the nozzle wall boundary layer. Thus the effective nozzle radius can vary depending on whether the boundary layer is fully laminar, transitions to turbulent within the nozzle, or is fully turbulent. The nominal value for this effective radius at the exit is $r_e = 0.02$ m which assumes laminar flow in the entire nozzle.

The SRQ of interest is the thrust force produced by the nozzle. The requirement is that the nozzle must produce a thrust of at least 2,600 N with 95% confidence for the nominal operating conditions shown in Table 1. The goal of the analysis is thus to determine whether one can have 95% confidence that the thrust produced by the nozzle will be greater than or equal to 2,600 N. The nozzle thrust is given by

$$Thrust = \left(\rho_e V_e^2 + p_e - p_\infty\right) A_e \tag{6}$$

where ρ_e, V_e, and A_e are the density, velocity, and area at the nozzle exit, respectively. The thrust produced by a deterministic simulation at the nominal conditions given in Table 1 and assuming a laminar boundary layer (i.e., $r_e = 0.02$ m) is 2,785.9 N, which is well above the required value of 2,600 N. We will now proceed to estimate the total uncertainty in the prediction of nozzle thrust by estimating uncertainty due to numerical approximations, model inputs, and the form of the model.

Table 1: Nominal nozzle boundary conditions.

Stagnation Pressure, p_o	6 MPa
Stagnation Temperature, T_o	300 K
Pressure of Surroundings, p_∞	0.101325 MPa

5.1 Numerical uncertainty

In order to estimate the numerical uncertainty, a grid refinement study was performed at the nominal conditions and assuming a laminar boundary layer in the entire nozzle. Computations were performed on six mesh levels as shown in Table 2. The computations were performed using double precision arithmetic and were iteratively converged down by 12 orders of magnitude from the initial level of the iterative residuals; thus round-off and iterative errors can be neglected. In addition, prior code verification studies showed that the numerical solutions converged to an exact solution at the formal order of accuracy of 2, providing confidence that there are no coding mistakes. The observed order of accuracy gives the rate at which estimated discretization error reduces with systematic mesh refinement [1,3]. For the current case, the observed order $\hat{p}$ was computed from

$$\hat{p} = \frac{\ln\left(\dfrac{Thrust_{coarse} - Thrust_{med}}{Thrust_{med} - Thrust_{fine}}\right)}{\ln(r)} \tag{7}$$

where $r = 2$ is the grid refinement factor. The observed order of accuracy was found to vary between 2.2 and 2.6. The formal order of accuracy of this finite volume discretization is 2, thus we can be reasonably confident that the solutions are in or near the asymptotic grid convergence range. Richardson extrapolation [1,3] was used along with the two finest mesh levels to estimate the exact solution as

$$Thrust_{exact} \approx Thrust_{fine} + \frac{Thrust_{fine} - Thrust_{med}}{r^p - 1} = 2815.417 \text{ N.}$$

The uncertainty due to numerical discretization is estimated by taking the absolute value of the error estimate and multiplying by a factor of safety of 1.25. The resulting uncertainty estimate due to discretization on the 64 cell mesh is

$$U_{NUM} = U_{DE} \cong 1.25 \left| Thrust_{64} - Thrust_{exact} \right| = 36.85 \text{ N.}$$

The uncertainty band in the thrust on the 64 cell mesh is 2,785.9 ± 36.8 N (or ±1.3%), which is deemed sufficiently accurate for the uncertainty propagation simulations. Although additional grid studies could be performed for different values of the model inputs, for simplicity, the above numerical uncertainty estimate will be applied for all cases.

Table 2: Number of mesh cells and predicted nominal thrust.

Grid Cells	Thrust (N)
512	2,815.19
256	2,814.51
128	2,810.31
64	2,785.94
32	2,670.87
16	1,903.09

5.2 Model input uncertainty

A simple sensitivity analysis showed that the thrust results were sensitive to the nozzle plenum (i.e., stagnation) pressure and the state of the nozzle side-wall boundary layer. Hypothetical experimental measurements showed that the actual nozzle stagnation pressures deviated from the nominal values for a given run. These variations were found to be distributed normally about the mean of 6 MPa with a standard deviation of 0.075 MPa. The stagnation pressure was thus chosen to be an aleatory uncertain model input and treated probabilistically. The laminar, transitional, or turbulent state of the nozzle side-wall boundary layer was unknown. However, separate boundary layer computations were performed assuming the boundary layer was either fully laminar or fully turbulent. When the boundary layer displacement thickness was accounted for, the effective test section exit radius was found to be 0.02 m for fully laminar flow and 0.016 m for fully turbulent flow. These two limits thus provide physically-based bounding values for the exit radius since the true value could be any possible value in this range if the flow transitions from laminar to turbulent at any point within the nozzle. Since absolutely no information is available as to which value is correct, the nozzle exit radius is an epistemic uncertainty and is characterized by an interval r_{exit} = [0.016, 0.02] m. All other model inputs are either assumed to be known precisely or shown to have little impact on the nozzle thrust.

Sampling is used to propagate the model input uncertainties through the model to determine their effects on the nozzle thrust. Monte Carlo sampling with 100 samples is used for the aleatory uncertain stagnation pressure. Latin hypercube sampling with 20 samples is used for the interval uncertain effective nozzle exit radius, where the interval is decomposed into 20 equally-space sub-intervals. Each sub-interval is randomly sampled using a uniform distribution except for the first and last sub-intervals, where probabilities of 0 and 1 are chosen, respectively, to ensure the interval endpoints are included.

Both of the approaches described above for segregated sampling of the probabilistic and interval uncertain inputs are investigated. In the first (E-outer), a sample is chosen for the interval uncertain input which will be used in the outer sampling loop. Then, all 100 random samples over the probabilistic input

are computed to produce a CDF conditioned on the interval value. A new interval uncertain input is then chosen and the process is repeated. The results of computing this ensemble of CDFs are shown in **FIG. 8**. A p-box can be formed by taking the outer extent of the ensemble of CDFs as shown in **FIG. 9**. Again, when the interval uncertain input is used in the outer loop of the segregated uncertainty propagation, then any advanced approach to uncertainty propagation can be used for the probabilistic inputs (polynomial chaos, stochastic collocation, etc.).

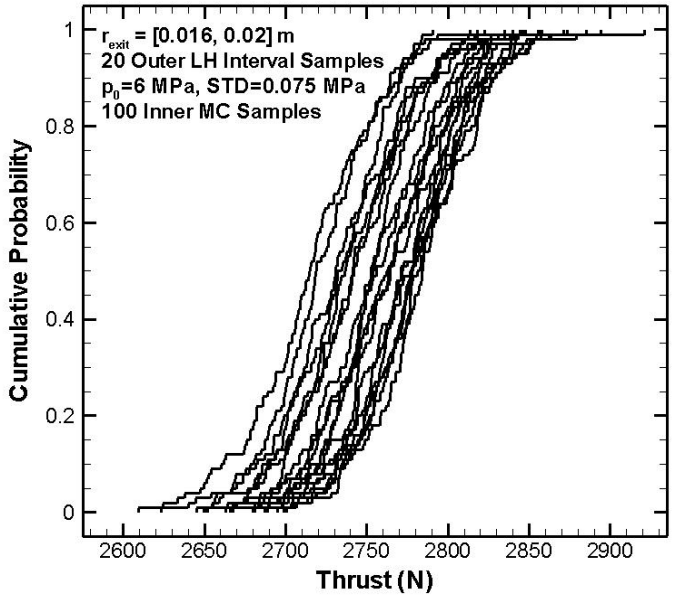

FIG. 8: Conditional CDFs generated by segregated sampling: outer loop is Latin hypercube sampling over the interval uncertain input and inner loop is Monte Carlo sampling over the probabilistic input.

The second approach to segregated uncertainty propagation (A-Outer) is also examined, where sampling over the probabilistic (aleatory uncertain) input is placed in the outer loop. For this case, sampling over the interval uncertain input is used on the inner loop in order to obtain an interval in the SRQ conditioned on the sample value for the random variable. However, advanced methods for interval propagation could also be used in this inner loop such as interval arithmetic or optimization techniques for determining minimum and maximum SRQ values. For each Monte Carlo sample of the probabilistic input, a new interval for the output SRQ is produced. Once the outer loop sampling is completed, the series of lower bounds of the SRQ are ordered from smallest to largest and form the left side of the p-box. The series of upper bounds of the SRQ are also ordered from smallest to largest and form the right side of the p-box. The p-box formed by sampling over the aleatory input in the outer loop (A-Outer) is also shown in **FIG. 9**. Note that for this case, the two p-boxes are similar and would likely converge to the same p-box in the limit of infinite samples. In addition, when accounting for only model input uncertainty (i.e., neglecting model form and numerical uncertainty), the minimum thrust requirement of 2,600 N is met with more than 95% confidence, at least within the limited number of samples.

Also shown in **FIG. 9** is the CDF that results from characterizing the epistemic uncertain input (effective nozzle exit radius) as a uniformly distributed probability over the interval bounds rather than an interval. When treated as a uniform probability over the interval range, the 95% confidence level for minimum thrust is 2688.8 N. This characterization assumes that all values in the interval for the effective nozzle exit radius are equally likely. However, as discussed previously, the state of the side-wall boundary layer is unknown: it could be fully laminar, transitional, or fully turbulent. The characterization of this epistemic uncertainty as an interval correctly represents possible values that the exit radius could take and results in a 95% confidence level that the achieved thrust will be in the interval [2647.6, 2714.4]

N. To ensure that a given minimum thrust level is achieved, it is the lower bound of this interval that must be used, i.e., 2647.6 N. Thus treating the interval uncertain input as a uniform probability overpredicts the minimum thrust by nearly 40 N. This overprediction would be even larger if a normal distribution was assumed with the interval bounds used for the $\pm 2\sigma$ values (i.e., with the interval bounds placed at plus and minus two standard deviations).

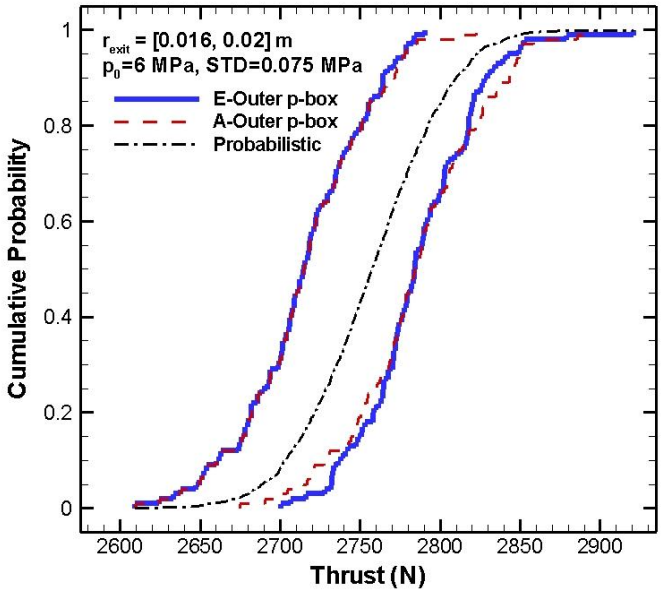

FIG. 9: P-boxes generated by segregated sampling: the blue solid line is the outer extend of the conditional CDFs found by using the interval uncertain input in the outer loop (E-Outer p-box) and the red dashed line is the p-box found by using the probabilistic (aleatory uncertain) input in the outer loop (A-Outer p-box). Also shown is the CDF that results from treating the epistemic uncertain input as a uniformly distributed probability over the interval (black dash-dot line).

5.3 Model form uncertainty

As discussed earlier, there are two steps in the estimation of the model form uncertainty: the computation of a validation metric and the extrapolation of the metric to the prediction conditions [1,2]. Comparisons between simulation and experiment are made at stagnation pressures that are sufficiently low that the nozzle side-wall boundary layer will be fully laminar. Thus the epistemic interval uncertainty due to the state of the nozzle boundary layer is eliminated and the only uncertain input is the stagnation pressure value. Since no actual experiments are run for this case, we will generate "synthetic" experimental data for illustrative purposes. Five measurements of the thrust are generated for a nominal stagnation pressure of 3 MPa by sampling from a normal distribution with a mean value of 1,330 N and a standard deviation of 60 N. These values are chosen to provide both a bias error relative to the simulation CDF and an increase in the standard deviation due to additional random errors when experimentally measuring the thrust. The CDFs from both the simulation and the experiment are given in **FIG. 10**, and the area validation metric (the area between the two CDFs) is computed from Eq. (4). For this case, the area validation metric is computed as 28.8 N and reflects the evidence for disagreement between the thrust predicted by the simulation and that measured in the experiment at these conditions.

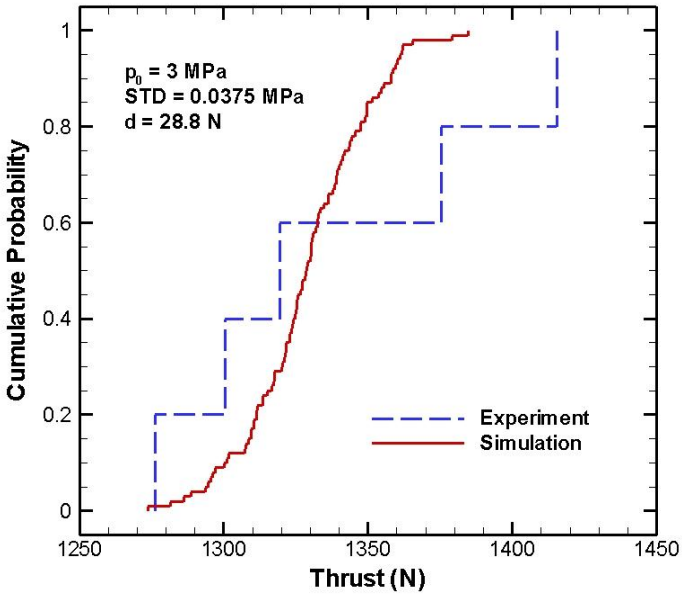

FIG. 10: CDFs from the simulation and experiment for a stagnation pressure of 6 MPa; the area between the two CDFs is the area validation metric.

Additional area validation metrics are computed from simulations and "synthetic" experiments at stagnation pressures of 1.0, 1.5, 2.0, and 2.5 MPa, yielding metrics of 23.0, 25.0, 24.0, and 26.2 N, respectively. These validation metrics represent estimated model form uncertainty for stagnation pressure values between 1.0 and 3.0 MPa. If the prediction conditions were within this range, say at 1.8 MPa, then model calibration (e.g., based on Bayesian updating) may be appropriate. However, since the prediction condition (6 MPa) is well outside this range, we instead choose to estimate the uncertainty at the prediction conditions using the current model. In order to extrapolate this model form uncertainty to the prediction condition, we first compute a linear regression fit of the area validation metric as a function of the stagnation pressure. The resulting regression fit is

$$\hat{d} = 20.28 + 2.56 p_0 \quad N \tag{8}$$

with p_0 given in MPa. The computed values of the area validation metric, along with the above regression fit, are shown graphically in **FIG. 11**. Prediction intervals for the regression fit [26] are then computed which provide the expected 95% confidence level between the simulation predictions and future experimental measurements of the thrust (see **FIG. 11**) and are given by

$$\hat{d} \pm t_{\alpha/2,N-df}\, s \sqrt{1 + \frac{1}{N} + \frac{N(p_0 - \bar{p}_0)^2}{N\sum_N p_{0,i}^2 - \left(\sum_N p_{0,i}\right)^2}}\,. \tag{9}$$

Here N is the number of validation experiments conducted (N = 5), p_0 is the stagnation pressure where we wish to estimate the prediction interval (p_0 = 6 MPa), $t_{\alpha/2,N-d}$ is the 1-$\alpha/2$ quantile of the student's t distribution for the degrees of freedom df (here df = 2 since there are two parameters in the regression fit

and for the two-sided 95% interval $t_{95\%,1}$ = 12.71), and s is the square root of the mean square error of the regression fit

$$s = \left[\frac{\sum_{i=1}^{N} \left(d_i - \hat{d}_i \right)^2}{N-2} \right]^{1/2} = 1.11 \text{ N.}$$

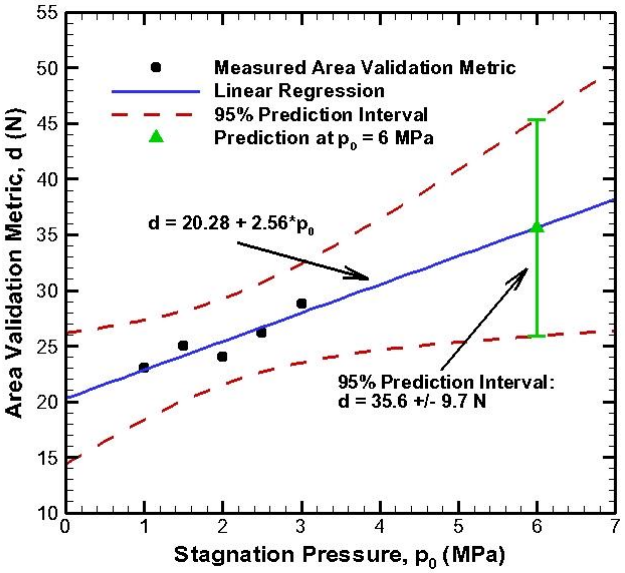

FIG. 11: Extrapolation of area validation metric to the prediction conditions (p_0 = 6 MPa) including prediction intervals.

The upper value of the prediction interval is then used to estimate the model form uncertainty at the prediction conditions where no experimental data are available. In this case, the regression fit of the validation metric evaluated at the prediction conditions (6 MPa) gives $\hat{d} = 35.6$ N. The magnitude of the 95% prediction interval at this location is P = ±9.7 N (i.e., $\hat{d} \pm P$). Thus the estimated model form uncertainty U_{MODEL} is

$$U_{MODEL} = \max(\hat{d}, 0) + P = 35.6 + 9.7 \text{ N} = 45.3 \text{ N.}$$

Since this estimated model form uncertainty is epistemic in nature, it is treated as an interval about the simulation prediction. For the simple case where there are no model input or numerical uncertainties, this model form uncertainty is simply added as an interval about the simulation prediction value. For example, if the simulation prediction is ThrustSIM = 2757.5 N, then the resulting interval accounting for model form uncertainty is

$$Thrust_{SIM} \pm U_{MODEL} = 2757.5 \pm 45.3 \text{ N.}$$

For the more realistic case where the model input uncertainties result in a CDF (or a p-box) of the SRQ, then this model form uncertainty is added as an interval to each side of the CDF (or the p-box). This process will be shown graphically in the next section.

5.4 Total prediction uncertainty

The total prediction uncertainty is now found by combining the propagated uncertainty from the model inputs (aleatory and epistemic) with the uncertainty due to the form of the model and the numerical approximations. The p-box that was generated by propagating the model input uncertainties through the model at a nominal stagnation pressure of 6 MPa (recall **FIG. 9**) can now be extended to reflect the estimated model form and numerical uncertainties. For example, if $F(x)$ is the CDF resulting from propagating random uncertainties through a model, then accounting for the model form and numerical uncertainties would result in the p-box $F(x \pm U_{TOTAL})$ where $U_{TOTAL} = U_{MODEL} + U_{NUM}$. In the current case, the propagation of the aleatory and epistemic uncertainties through the model results in a p-box. The uncertainties due to model form and numerical approximations simply result in a broadening of this p-box. This "extended" p-box is shown in **FIG. 12**. While the minimum thrust of 2,600 N is met when only the model input uncertainties are considered, when the additional model form and numerical uncertainties are included, there is a 22% chance that the thrust will be below the required 2,600 N. Stated another way, we can only have 78% confidence that the minimum thrust requirement will be met.

The holistic approach to quantifying uncertainty shown in **FIG. 12** provides a significant amount of information to a decision maker regarding both the magnitude and sources of uncertainty in the M&S predictions. The numerical uncertainty could be reduced by approximately a factor of four by using a 128 cell mesh instead of a 64 cell mesh in the simulation. The epistemic uncertainties could be reduced or eliminated by measuring the location of laminar to turbulent transition in the nozzle. Finally, the model form uncertainty could be reduced by performing additional experiments at or near the prediction location. If the experimental data is used to improve the model, then additional experiments would be needed to estimate the model form uncertainty in the new (improved) model.

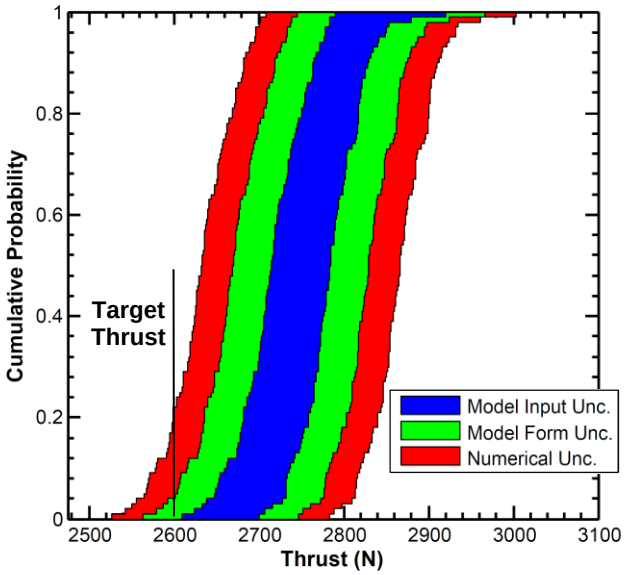

FIG. 12: Extended p-box for nozzle thrust accounting for propagation of model input uncertainty (blue), model form uncertainty (green), and numerical uncertainty (red).

By propagating the model input uncertainty through the model at different stagnation pressures, the 90% confidence limits (found from the 5% cumulative probability location on the left side of the original p-box and the 95% cumulative probability location on the right side of the p-box) for the thrust as a function of the stagnation pressure can be examined (see **FIG. 13**). Note that there is an increase in the width of these confidence bounds above 3 MPa where the additional epistemic (interval) uncertainty of the state of the nozzle boundary layer (i.e., the effective nozzle exit radius) is included. Also shown in the

figure are the 90% confidence bounds which include the addition of model form and numerical uncertainty (i.e., they are taken from the extended p-box). Note that the model form uncertainty grows as one get farther from the validation domain (recall the growth in the prediction intervals at higher stagnation pressures from **FIG. 11**).

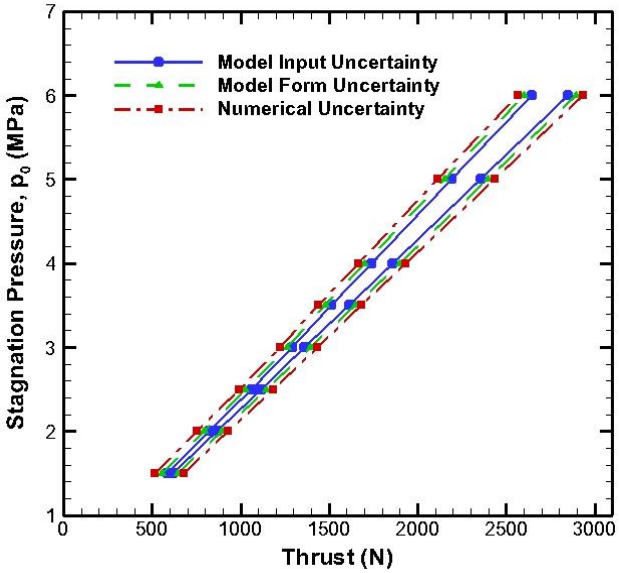

FIG. 13: 90% confidence bounds for thrust predictions as a function of stagnation pressure.

6. CONCLUSIONS

This article presents a holistic approach to uncertainty quantification. In addition to uncertainty in the model inputs, it accounts for uncertainties due to numerical approximations and the form of the model. Explicit inclusion of model form uncertainty is an alternative to simply ignoring it or to calibrating the model to remove it (e.g., Bayesian updating). Calibration/model updating may be appropriate when experimental data are plentiful for the system of interest and the prediction location lies within the validation domain. However, for practical applications, one is often faced with 1) sparse data, 2) data for simpler systems, 3) data on vaguely similar systems, or even 4) no data at all. For these cases, we feel it is better to quantify the model form uncertainty with the available data and make it available to the decision maker along with the other uncertainty sources present (recall **FIG. 12**). For the example problem given in Section 5, the goal was to see if a minimum nozzle thrust of 2,600 N could be achieved with 95% confidence. Neglecting the model form and numerical uncertainties led to a minimum thrust level of 2647.6 N which met the thrust requirement, whereas the minimum thrust accounting for these additional uncertainty sources was 2565.5 N which did not meet the requirement.

The importance of the proper treatment of epistemic (lack of knowledge) uncertainties was also discussed. While it is common practice to treat epistemic uncertainties as random variables with uniform (or normal) distributions, when little is known about the value of an epistemic uncertainty, a probabilistic treatment is not justified and an interval characterization is appropriate. In the simple examples of Section 4, the probabilistic characterization of epistemic uncertainty was shown to greatly underpredict the uncertainty in the output relative to interval treatment. In the more complex M&S example of Section 5, treating the epistemic uncertainty as a uniform random variable also underpredicted the uncertainty (recall **FIG. 9**), overpredicting the minimum thrust by nearly 40 N.

When both interval-valued and probabilistic model input uncertainties are present, then segregated uncertainty propagation is needed. Two approaches to segregated propagation were discussed which differed depending on whether the interval-uncertain inputs or the probabilistic inputs were used in the

outer loop. When the interval-uncertain model inputs were sampled in the outer loop, the result for the SRQ (in the limit of infinite samples) was a p-box that was correct when independence was assumed between input uncertainties. With this approach, the (inner loop) propagation of the random uncertainties can be performed with any technique (sampling, polynomial chaos, stochastic collocation, etc.). When the probabilistic model inputs were sampled in the outer loop, the result for the SRQ (in the sampling limit) was a (possibly larger) p-box that was correct when the dependence between uncertain inputs is unknown. With this second approach, the propagation of the interval-uncertain inputs through the model could be performed with any technique (sampling, interval arithmetic, optimization, etc.).

References

1. Oberkampf, W. L. and C. J. Roy (2010). *Verification and Validation in Scientific Computing*, Cambridge University Press, Cambridge.
2. Roy, C. J. and W. L. Oberkampf (2011). "A Comprehensive Framework for Verification, Validation, and Uncertainty Quantification in Scientific Computing," *Computer Methods in Applied Mechanics and Engineering*, Vol. 200, Nos. 25-28, pp. 2131-2144 (DOI: 10.1016/j.cma.2011.03.016).
3. Roache, P. J. (2009). *Fundamentals of Verification and Validation*, Hermosa Publishers, Socorro, New Mexico.
4. AIAA (1998). *Guide for the Verification and Validation of Computational Fluid Dynamics Simulations*, American Institute of Aeronautics and Astronautics, AIAA-G-077-1998, Reston, VA.
5. ASME (2006). *Guide for Verification and Validation in Computational Solid Mechanics*, American Society of Mechanical Engineers, ASME Standard V&V 10-2006, New York, NY.
6. Ferson, S., L.R. Ginzburg (1996). "Different Methods are Needed to Propagate Ignorance and Variability," *Reliability Engineering and System Safety*, Vol. 54, pp. 133-144.
7. Cooke, R. M. (1991). *Experts in Uncertainty: Opinion and Subjective Probability in Science*, Oxford University Press, New York.
8. Ghosh, J. K., M. Delampady, and T. Samanta (2006). *An Introduction to Bayesian Analysis: Theory and Methods*, Springer, Berlin.
9. Hu, C., Kearfott, R. B., de Korvin, A., and Kreinovich, V. (2008). *Knowledge Processing with Interval and Soft Computing*, Springer-Verlag, London.
10. Shafer, G. A. (1976). *Mathematical Theory of Evidence*, Princeton University Press, Princeton, NJ.
11. Ferson, S., V. Kreinovich, L. Ginzburg, D. Myers, and K. Sentz (2003). Constructing Probability Boxes and Dempster-Shafer Structures. Technical Report for Sandia National Labs. SAND2002-4015. January 2003.
12. Zaffalon, M. (2002), "The Naïve Credal Classifier," *Journal of Statistical Planning and Inference*, Vol. 101, No. 1, pp. 5-21.
13. Balch, M. (2010). Methods for Rigorous Uncertainty Quantification with Application to a Mars Atmosphere Model, Doctoral Thesis, Virginia Tech, November 2010.
14. Joslyn, C. and S. Ferson (2005). "Approximate Representations of Random Intervals for Hybrid Uncertainty Quantification in Engineering Modeling." *Sensitivity Analysis of Model Output*. K Hanson and F Hemez, eds. Los Alamos National Laboratory (http://library.lanl.gov)
15. Fishman, G. S. (1995). *Monte Carlo: Concepts, Algorithms, and Applications*, Springer, New York.
16. Xiu, D. (2010). *Numerical Methods for Stochastic Computations: A Spectral Method Approach*, Princeton University Press, Princeton, NJ.
17. Ghanem, R. G. and P. D. Spanos (1991). *Stochastic Finite Elements: A Spectral Approach*, Springer-Verlag, New York.

18. Hosder, S. and Walters, R. W., "Non-Intrusive Polynomial Chaos Methods for Uncertainty Quantification in Fluid Dynamics," AIAA Paper 2010-129, 48th AIAA Aerospace Sciences Meeting, 4 - 7 January, 2010, Orlando, FL.
19. Helton, J.C. (1997). "Uncertainty and sensitivity analysis in the presence of stochastic and subjective uncertainty," *Journal of Statistical Computation and Simulation*, Vol. 57, pp. 3-76.
20. Moore, R. E., R. B. Kearfott, and M. J. Cloud (2009). *Introduction to Interval Analysis*, Society for Industrial and Applied Mathematics, Philadelphia, PA.
21. Rump, S. M. (1999). "INTLAB - INTerval LABoratory." In Tibor Csendes, editor, *Developments in Reliable Computing*, pp. 77-104. Kluwer Academic Publishers, Dordrecht.
22. Phillips, T. S. and Roy, C. J. (2011). "Evaluation of Extrapolation-Based Discretization Error and Uncertainty Estimators," AIAA Paper 2011-215, 49th AIAA Aerospace Sciences, Jan. 4-7, 2011, Orlando, Florida.
23. Ferson, S., W. L. Oberkampf, and L. Ginzburg (2008). "Model validation and predictive capability for the thermal challenge problem." *Computer Methods in Applied Mechanics and Engineering*, 197, pp. 2408-2430.
24. Ferson, S., V. Kreinovich, J. Hajagos, W. Oberkampf, and L. Ginzburg (2007). Experimental Uncertainty Estimation and Statistics for Data Having Interval Uncertainty. Technical Report for Sandia National Labs. SAND2007-0939. May 2007.
25. Ferson, S., R. Nelsen, J. Hajagos, D. Berleant, J. Zhang, W. Tucker, L. Ginzburg, and W. Oberkampf (2004). Dependence in probabilistic modeling, Dempster-Shafer theory, and probability bounds analysis. Technical Report for Sandia National Labs. SAND2004-3072. October 2004.
26. Devore, J., (2009). *Probability and Statistics for Engineering and the Sciences*, 7th Ed., Brooks/Cole, Belmont, CA.